J|A|C|S
ARTICLES
Published on Web 01/10/2006

Growth Kinetics of Heterostructured GaP−GaAs Nanowires

Marcel A. Verheijen,[†] George Immink,[†] Thierry de Smet,[†,‡]
Magnus T. Borgström,[†] and Erik P. A. M. Bakkers*[,†]

Contribution from Philips Research Laboratories and Cedova, Professor Holstlaan 4, 5656 AA Eindhoven, The Netherlands

Received October 20, 2005; E-mail: erik.bakkers@philips.com

Abstract: We have studied the vapor−liquid−solid (VLS) growth dynamics of GaP and GaAs in heterostructured GaP−GaAs nanowires. The wires containing multiple GaP−GaAs junctions were grown by the use of metal−organic vapor phase−epitaxy (MOVPE) on SiO_2, and the lengths of the individual sections were obtained from transmission electron microscopy. The growth kinetics has been studied as a function of temperature and the partial pressures of the precursors. We found that the growth of the GaAs sections is limited by the arsine (AsH_3) as well as the trimethylgallium ($Ga(CH_3)_3$) partial pressures, whereas the growth of GaP is a temperature-activated, phosphine(PH_3)-limited process with an activation energy of 115 ± 6 kJ/mol. The PH_3 kinetics obeys the Hinshelwood−Langmuir mechanism, indicating that the dissociation reaction of adsorbed PH_3 into PH_2 and H on the catalytic gold surface is the rate-limiting step for the growth of GaP. In addition, we have studied the competitive thin layer growth on the sidewalls of the nanowires. Although the rate of this process is 2 orders of magnitude lower than the growth rate of the VLS mechanism, it competes with VLS growth and results in tapered nanowires at elevated temperatures.

Introduction

Semiconducting nanowires are one of the most promising materials for the monolithic integration of high-performance semiconductors with silicon technology.[1−3] These nanowires are grown by the vapor−liquid−solid (VLS) mechanism,[4] and devices such as field-effect transistors,[5] logic gates,[6] and supercurrent switches[7] have been fabricated. The electronic properties of these wires are, to a large extent, controlled by the chemical composition and by impurity dopants.[8] However, when the radius of the wires becomes very small, typically <10 nm, size quantization effects start to play a role.[9] For the fabrication of optical or electrical devices, local variations in the electronic structure of the wire, such as heterojunctions, are required. Nanowires, in which the chemical composition was varied in the longitudinal direction, have been fabricated from semiconductors, such as Si−Ge,[10] and from several compound semiconductors, like GaAs−InAs,[11] InP−InAs,[12] GaN−AlGaN,[13] and GaP−GaAs.[14] If the segments are very short (<10 nm), size quantization will occur, and this has been observed electrically[15] as well as optically.[16] For any application, control over the growth rates of the individual materials in such heterostructured nanowires is desired since the optoelectronic properties of the sections critically depend on their dimensions in the nanometer regime. So far, the VLS growth kinetics has been evaluated from the total length of wires,[17−22] epitaxially grown on corresponding substrates. In such studies, competitive thin film deposition or catalytic processes on the crystalline substrate surface often affect the VLS process. This disturbs an unambiguous investigation of the reactions taking place on the surface or inside the catalytic metal particle.

[†] Philips Research Laboratories.
[‡] Cedova.

(1) Kamins, T. I.; Li, X.; Williams, R. S.; Liu, X. *Nano Lett.* **2004**, *4*, 503−506.
(2) Bakkers, E. P. A. M.; van Dam, J. A.; De Franceschi, S.; Kouwenhoven, L. P.; Kaiser, M.; Verheijen, M. A.; Wondergem, H.; van der Sluis, P. *Nat. Mater.* **2004**, *3*, 769−773.
(3) Mårtensson, T.; Svensson, C. P. T.; Wacaser, B. A.; Larsson, M. W.; Seifert, W.; Deppert, K.; Gustafsson, A.; Wallenberg, L. R.; Samuelson, L. *Nano Lett.* **2004**, *4*, 1987−1990.
(4) Wagner, R. S.; Ellis, W. C. *Appl. Phys. Lett.* **1964**, *4*, 89−90.
(5) De Franceschi, S.; van Dam, J. A.; Bakkers, E. P. A. M.; Feiner, L. F.; Gurevich, L.; Kouwenhoven, L. P. *Appl. Phys. Lett.* **2003**, *83*, 344−346.
(6) Huang, Y.; Duan, X.; Cui, Y.; Lauhon, L. J.; Kim, K.-H.; Lieber, C. M. *Science* **2001**, *294*, 1313−1317.
(7) Doh, Y.-J.; van Dam, J. A.; Roest, A. L.; Bakkers, E. P. A. M.; Kouwenhoven, L. P.; De Franceschi, S. *Science* **2005**, *309*, 272−275.
(8) Haraguchi, K.; Katsuyama, K.; Hiruma, K.; Ogawa, K. *Appl. Phys. Lett.* **1992**, *60*, 745−747.
(9) Gudiksen, M. S.; Wang, J.; Lieber, C. M. *J. Phys. Chem.* **2002**, *106*, 4036−4039.
(10) Wu, Y.; Fan, R.; Yang, P. *Nano Lett.* **2002**, *2*, 83−86.
(11) Hiruma, K.; Murakoshi, H.; Yazawa, M.; Katsuyama, T. *J. Cryst. Growth* **1996**, *163*, 226−231.
(12) Björk, M. T.; Ohlsson, B. J.; Sass, T.; Persson, A. I.; Thelander, C.; Magnusson, M. H.; Deppert, K.; Wallenberg, L. R.; Samuelson, L. *Nano Lett.* **2002**, *2*, 87−89.
(13) Ristic, J.; Sanchez-Garcia, M. A.; Calleja, E.; Sanchez-Paramo, J.; Calleja, J. M.; Jahn, U.; Ploog, K. H. *Phys. Stat. Sol. (a)* **2002**, *192*, 60−66.
(14) Gudiksen, M. S.; Lauhon, L. J.; Wang, J.; Smith, D. C.; Lieber, C. M. *Nature* **2002**, *415*, 617−620.
(15) Björk, M. T.; Thelander, C.; Hansen, A. E.; Jensen, L. E.; Larsson, M. W.; Wallenberg, L. R.; Samuelson, L. *Nano Lett.* **2004**, *4*, 1621−1625.
(16) Borgström, M. T.; Zwiller, V.; Müller, E.; Imamoglu, A. *Nano Lett.* **2005**, *5*, 1439−1443.
(17) Bootsma, G. A.; Gassen, H. J. *J. Cryst. Growth* **1971**, *10*, 223.
(18) Givargizov, E. I. *J. Cryst. Growth* **1975**, *31*, 20.
(19) Jensen, L. E.; Björk, M. T.; Jeppesen, S.; Persson, A. I.; Ohlsson, B. J.; Samuelson, L. *Nano Lett.* **2004**, *4*, 1961−1964.
(20) Dick, K. A.; Deppert, K.; Mårtensson, T.; Mandl, B.; Samuelson, L.; Seifert, W. *Nano Lett.* **2005**, *5*, 761−764.
(21) Persson, A. I.; Ohlsson, B. J.; Jeppesen, S.; Samuelson, L. *J. Cryst. Growth* **2004**, *272*, 167−174.
(22) Borgström, M.; Deppert, K.; Samuelson, L.; Seifert, W. *J. Cryst. Growth* **2004**, *260*, 18−22.

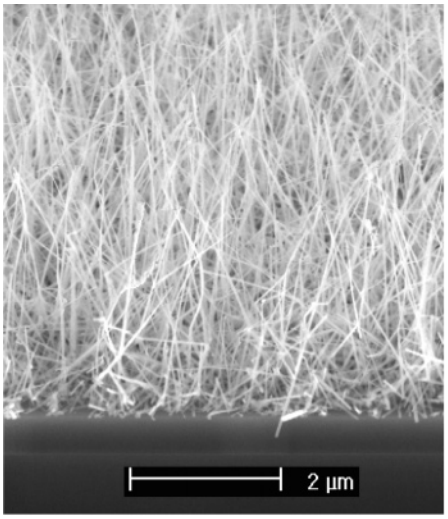

Figure 1. SEM image of heterostructured GaP−GaAs nanowires grown on a thermally oxidized Si substrate.

In this paper, the growth dynamics of GaP−GaAs nanowires, with multiple heterojunctions, synthesized with metal−organic vapor phase−epitaxy (MOVPE) has been studied. The growth of multi-segmented GaP−GaAs nanowires enables to study the individual contribution of the group III and V precursors to the VLS growth. The growth rates were determined accurately by measuring the lengths of the alternating segments with transmission electron microscopy (TEM). The wires have been grown on inert SiO_2 surfaces, such that material deposition at the substrate surface is suppressed. This enables to study the catalytic action of the metal particle. Although the material deposition on the SiO_2 substrate surface was frustrated, growth of a thin film on the sidewalls of the nanowires occurs at elevated temperatures. We were able to study this competitive reaction in detail since the heterostructures offer a precise internal time reference, such that exposure times at specific positions on the wires could be accurately determined afterward with TEM.

Experimental Procedures

Substrates for the wire growth were prepared by dispersing Au colloids (diameter of 20 nm) on a thermally oxidized (500 nm) silicon substrate. The nanowires were synthesized in an Aixtron 200 MOVPE reactor from $(CH_3)_3Ga$ (trimethylgallium, TMG), PH_3, and AsH_3 precursors in H_2 at a total pressure of 50 mbar in a total flow of 6.0 L/min (slm). The TMG molar fraction (χ_{TMG}) was in the range of 1.5×10^{-5} to 1.5×10^{-4}, and the PH_3 and AsH_3 molar fractions were varied in the range of 7.5×10^{-4} to 5.0×10^{-2}. During heating of the substrate, a PH_3 pressure was applied, and when the desired growth temperature was reached, growth was initiated by opening the TMG source. The first segment of the wire was a GaP segment, grown for 4 min. The heterojunctions were defined by the switching of the group V precursors. The growth time of the consecutive GaAs segments was decreased (120, 60, 30, 15, and 5 s), while that of the GaP parts was kept constant at 60 s. The resulting nanowire density was estimated from SEM studies (see Figure 1) to be around 10^{10} cm^{-2}.

All samples were studied with a Tecnai 300 keV TEM in both bright-field as well as in high-angle annular dark field (HAADF) mode. The chemical composition of the wires was studied using scanning TEM in combination with energy-dispersive X-ray analysis (EDX).

All wires were terminated by a Au particle and were grown in the ⟨111⟩ direction, as determined from high-resolution TEM studies.

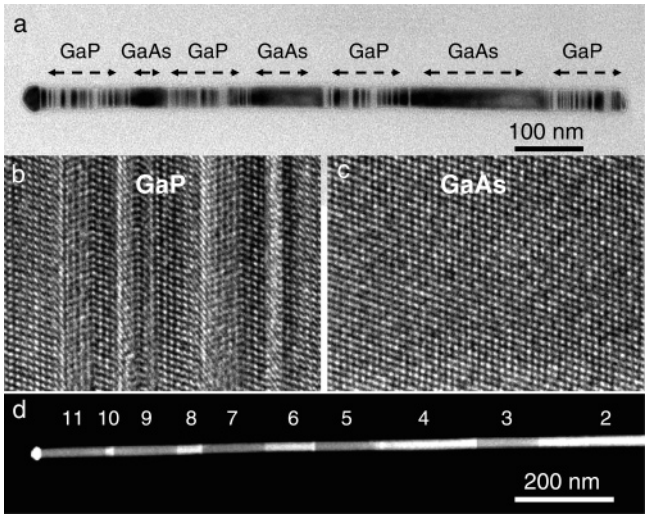

Figure 2. (a) Bright-field transmission electron microscopy (TEM) image of a heterostructured GaP−GaAs nanowire. The wire was grown at $T =$ 420 °C, and χ_{AsH3} and χ_{PH3} were 1.5×10^{-2}, and $\chi_{TMG} = 7.3 \times 10^{-5}$. The arrows indicate the segments. Rotational twin dislocations are present in the GaP sections (vertical contrast lines) but not in the GaAs parts. In the insets, typical high-resolution TEM images of a (b) GaP and (c) GaAs segment are shown. (d) HAADF TEM image of a wire grown at 420 °C but with $\chi_{AsH3} = 3.0 \times 10^{-3}$ visualizing the heterostructure. Since As is a heavier element than P, the GaAs sections give a brighter contrast than the GaP parts.

Samples for cross-sectional TEM imaging were prepared by wiping the as-grown sample over a Si substrate, resulting in a rough alignment of the transferred wires due to the shear forces. These horizontal wires were mechanically fixed by depositing a 50 nm SiO_2 layer on top by plasma-enhanced chemical vapor deposition. A thin vertical slice, oriented orthogonal to the length direction of the wires, was cut out by the use of an FEI FIB200 focused-ion beam from an area with a high density of wires.

Results and Discussion

Determination of Growth Rates. The TEM image in Figure 2a shows a heterostructured GaP−GaAs nanowire synthesized at 420 °C. The positions of the GaP and GaAs segments are indicated with arrows. The contrast lines, orthogonal to the length direction of the wire, within the GaP segments correspond to twin domains with alternating orientations along the long [111] axis of the wire. Surprisingly, the GaAs segments do not show these stacking faults at all. High-resolution TEM imaging clearly shows the stacking faults in the GaP segment (Figure 2b) and the single-crystalline nature of the GaAs section (Figure 2c). The defect density in the GaP and the crystallinity of the GaAs sections were neither affected by the temperature nor by changing the precursor partial pressures. This structural difference between the GaAs and the GaP sections allows fast estimation of the segment lengths in these structures. Figure 2d shows a HAADF (high-angle annular dark field) image of wire grown at the same temperature, but with $\chi_{AsH3} = 3.0 \times 10^{-3}$. The gold particle at the end of the wire and the GaAs sections are brighter than the GaP due to their higher average atomic number. The exact length of the sections, L, was determined from HAADF brightness profiles. For example, the length of a GaAs section, L_{GaAs}, was defined as the distance between the onset of the brightness increase and the onset of the fall of brightness because these changes in brightness correspond to switching of the AsH_3 and PH_3 sources. An EDX line scan was taken along the length direction of the wire.

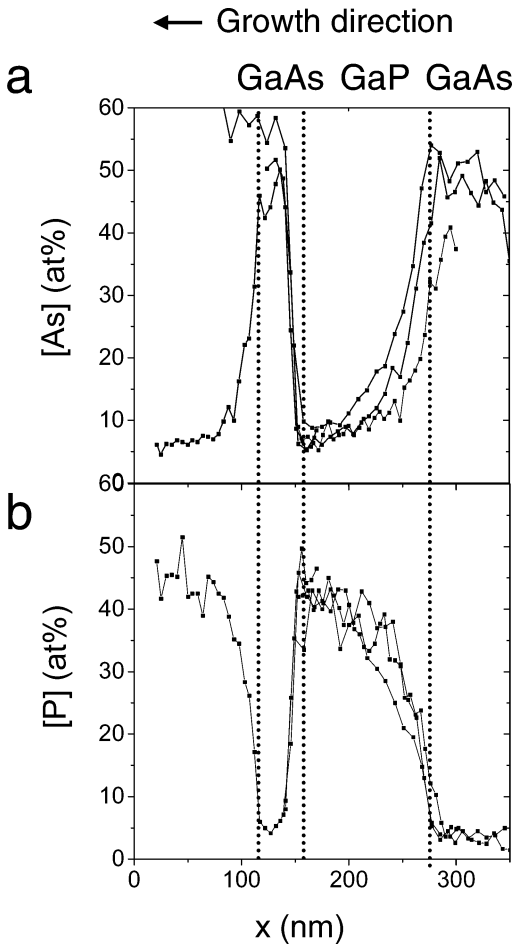

Figure 3. Energy-dispersive X-ray analysis (EDX) line scans of three consecutive GaAs−GaP−GaAs junctions of a wire from the same sample as in Figure 2a are plotted, such that the GaP sections overlap. (a) As concentration and (b) P concentration are plotted as a function of position. The growth direction was from right to left.

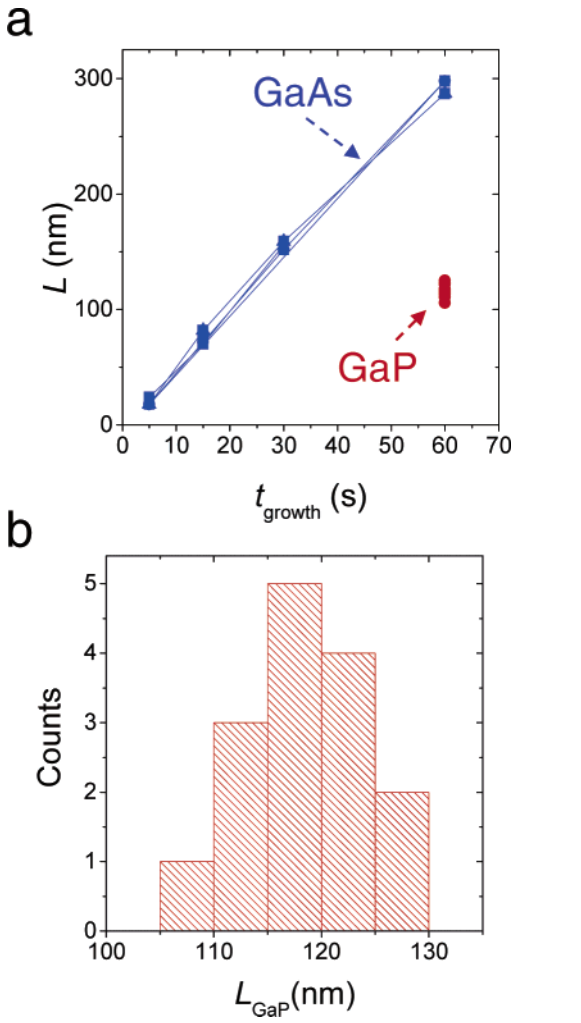

Figure 4. (a) Length of the GaAs and GaP sections of a wire from the same sample as in Figure 2a vs growth time. (b) Histogram of L_{GaP}.

In Figure 3, the EDX profiles for As and P, taken from three different parts of the wire, are plotted such that the GaP sections overlap. From these plots, the similarity in the compositional gradients at the different junctions is clear. The junction formed by growing GaAs on a GaP is quite sharp, while the junction formed by stacking GaP onto GaAs is gradual. The sharpness of the gradual junction was investigated in more detail and will be published elsewhere. In Figure 4a, L_{GaAs} and L_{GaP}, obtained from HAADF studies, for a number of wires grown at 420 °C ($\chi_{TMG} = 7.3 \times 10^{-5}$ and χ_{AsH3} and $\chi_{PH3} = 1.5 \times 10^{-2}$) were plotted versus the growth time. The growth rate of GaAs, R_{GaAs}, was taken from a linear fit to the data points. From the histogram plotted in Figure 4b, a deviation of ±10% in L_{GaP} was obtained, probably related to nonuniformities in the processing. The resulting crystal growth rates at 420 °C are $R_{GaP} = 1.8 \pm 0.2$ nm/s and $R_{GaAs} = 5.0 \pm 0.4$ nm/s.

Growth Rate versus Temperature. To study the growth kinetics in more detail, the heterostructured wires have been grown at different temperatures in the range of 400−520 °C, while the other growth parameters were kept constant ($\chi_{TMG} = 7.3 \times 10^{-5}$ and χ_{AsH3} and $\chi_{PH3} = 1.5 \times 10^{-2}$). In Figure 5a,b, R_{GaP} and R_{GaAs} have been plotted logarithmically versus $1000/T$ (Arrhenius plot). Each point in the graph was obtained by measuring at least 15 wire segments with TEM. The graph shows that R_{GaP} increases exponentially, from 1.2 to 19 nm/s, in the temperature range from 400 to 500 °C, and then decreases to 12 nm/s at 520 °C. R_{GaAs} is constant (~5.5 ± 0.5 nm/s) in the temperature range between 400 and 460 °C and then decreases to 1.5 nm/s at 500−520 °C.

Considering the VLS mechanism in combination with the MOVPE precursor molecules (see Figure 6), we can identify the following processes: (1) gas-phase diffusion, (2) dissociation reactions on the catalyst particle or on the nanowire surface, (3) diffusion of reactants through the catalyst particle,[23] (4) the formation of the semiconductor crystal at the liquid−solid interface, (5) adsorption of precursor molecules on the substrate or nanowire surface, (6) surface diffusion,[19] (7) crystal growth on the nanowire sidewall, and (8) film growth on the substrate surface. Steps 2, 4, 7, and 8 are activated processes, which depend exponentially on the temperature. The experiments show that the growth of GaP is dominated by a thermally activated process, with an activation energy of 115 ± 6 kJ/mol. For the VLS growth of GaP, it implies that either step 2 or 4 is rate limiting. If step 4 would be rate limiting, the growth rate should be independent of the precursor partial pressures. For GaAs, the growth rate is governed by a temperature independent parameter, indicating diffusion-limited growth, where growth rate varies with input flow.

(23) Bakkers, E. P. A. M.; Verheijen, M. A. *J. Am. Chem. Soc.* **2003**, *125*, 3440−3441.

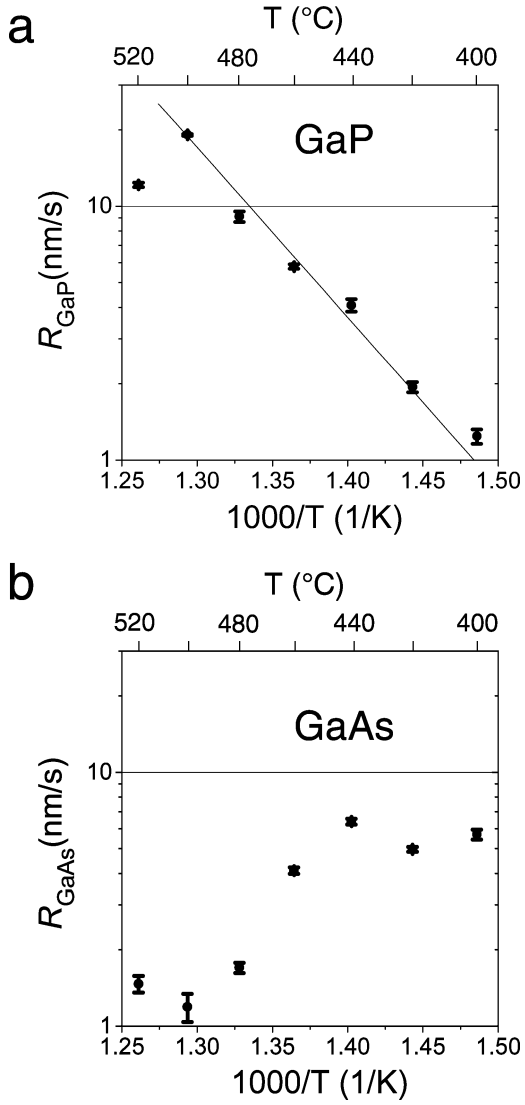

Figure 5. (a) R_{GaP} vs 1000/T on a semilogarithmic scale and (b) R_{GaAs} vs 1000/ T on a semilogarithmic scale. χ_{AsH3} and χ_{PH3} were 1.5×10^{-2}, and χ_{TMG} was 7.3×10^{-5} for these samples.

The decrease of R_{GaAs} (above 440 °C) and R_{GaP} (above 500 °C) with increasing temperature is due to the competitive growth (step 7) on the nanowire sidewalls (we have seen no material deposition (step 8) on the SiO_2 surface with SEM), as will be discussed in more detail next. Such a decrease in growth rate with increasing temperatures has previously been observed for GaAs wires grown on As-terminated-GaAs(111) substrates.[21,22] This effect was attributed to the competitive thin film deposition of GaAs on the substrate (step 8) and on the nanowire surface (step 7). In the parameter range used by these authors, however, the wire growth kinetics were not dominated by reactions on the catalytic particle or on the nanowire surface but rather by the decomposition of a group III precursor and GaAs deposition on the crystalline substrate.

Growth Rate versus Partial Gas Pressures. To determine which process is the rate-limiting step for the growth of GaP, and what precursor limits the GaAs growth, the growth rates were determined for different molar fractions, χ, of AsH_3, PH_3, and TMG. In Figure 7, R_{GaAs} and R_{GaP} are plotted versus χ_{TMG}. It is clear that R_{GaAs} strongly increases with χ_{TMG}, whereas R_{GaP} is hardly affected by a change in the TMG vapor concentration.

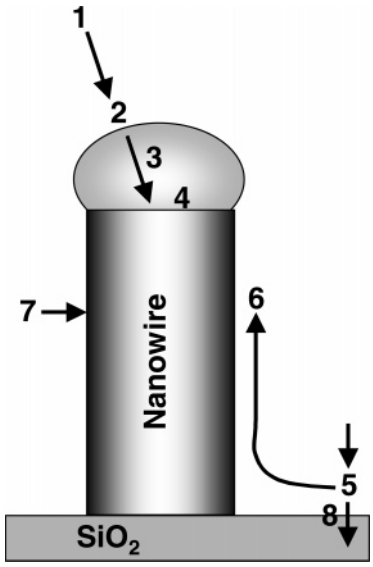

Figure 6. Schematic drawing of the relevant chemical processes in the nanowire growth. (1) Mass transport through the gas phase. (2) Dissociation reaction on the catalytic particle or on the nanowire surface. (3) Diffusion of reactants through the metal particle. (4) Formation of the semiconductor lattice at the liquid−solid interface. (5) Adsorption of precursor molecules on the substrate or nanowire surface. (6) Surface diffusion. (7) Film growth on the nanowire sidewall. (8) Film growth on the substrate surface.

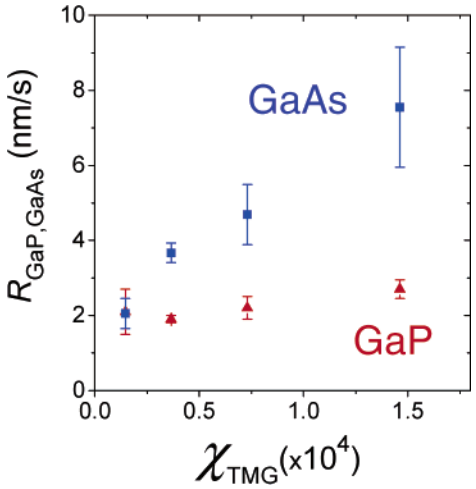

Figure 7. R_{GaP} and R_{GaAs} vs χ_{TMG}. The samples were grown at $T = 420$ °C, and χ_{AsH3} and χ_{PH3} were 1.5×10^{-2}.

The growth rate of GaP increases with χ_{PH3} (Figure 8a) and levels off at higher χ. When $1/k_{GaP}$ is plotted versus $1/\chi_{PH3}$ (Figure 8b), a linear relation is obtained. This relation complies with the classical Langmuir−Hinshelwood mechanism for unimolecular decomposition of adsorbates on a catalytic surface. The mechanism describes a first-order reaction at low χ and a zero-order reaction at high χ. This demonstrates that the thermally activated molecular dissociation of PH_3 (step 2) is the rate-determining step for GaP. Larsen et al.[24] have found that the pyrolysis of PH_3 strongly depends on the catalytic surface and that the rate-limiting process is the decomposition of adsorbed PH_3 into PH_2 (ads) and H (ads). The activation energy for this reaction on InP surfaces was 151 kJ/mol, which is significantly higher than the value we found, indicating that Au effectively catalyzes the decomposition of PH_3. It was shown

(24) Larsen, C. A.; Buchan, N. I.; Stringfellow, G. B. *J. Cryst. Growth* **1987**, *85*, 148−153.

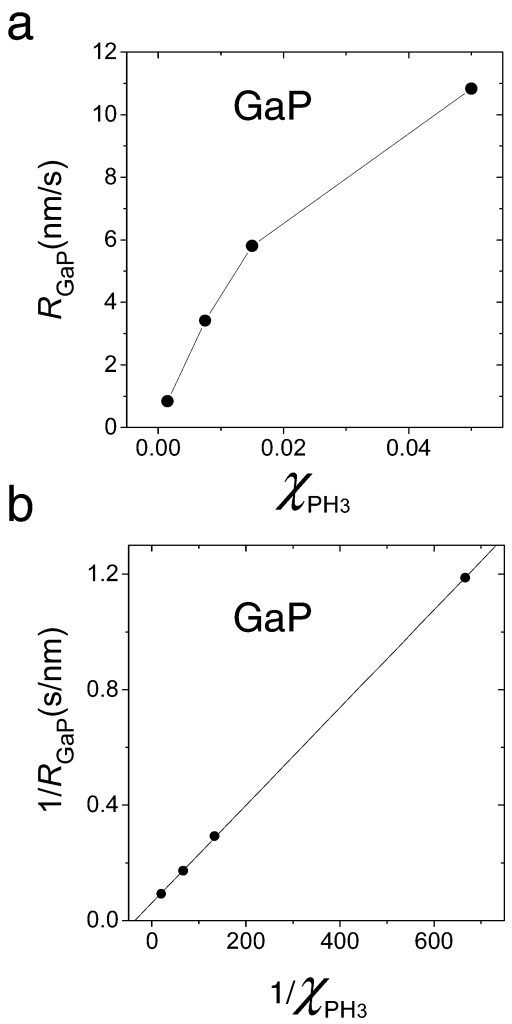

Figure 8. (a) R_{GaP} vs χ_{PH3}. The samples were grown at 460 °C with $\chi_{TMG} = 7.3 \times 10^{-5}$ and $\chi_{AsH3} = 1.5 \times 10^{-2}$. (b) Same data as in panel a but plotted as $1/R_{GaP}$ vs $1/\chi_{PH3}$. The solid line is a linear fit to the data.

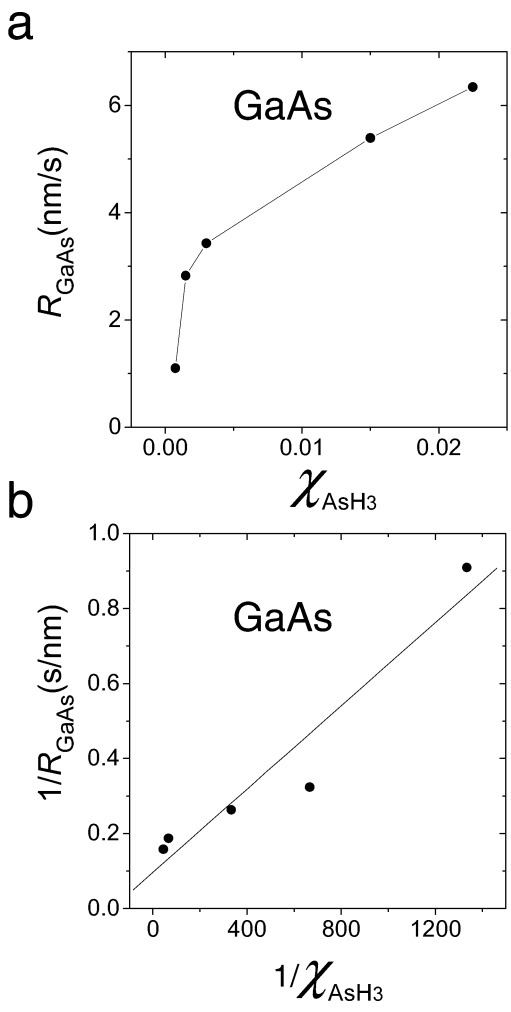

Figure 9. (a) R_{GaAs} vs χ_{AsH3}. Samples were grown at 420 °C with $\chi_{TMG} = 7.3 \times 10^{-5}$ and $\chi_{PH3} = 1.5 \times 10^{-2}$. (b) Same data as in panel a but plotted as $1/R_{GaAs}$ vs $1/\chi_{AsH3}$. The solid line is a linear fit to the data.

previously[17] that the catalyzed decomposition of the silane and germane precursors at the VL interface was the rate-limiting step for the VLS growth of silicon and germanium whiskers. To our best knowledge, our results represent the first experimental evidence for catalytic action of the metal particle in VLS growth of III−V nanowires (i.e., lowering of activation energy).

The results for GaAs wire growth indicate diffusion-limited growth, as is typically observed by MOVPE, where the growth rate is usually controlled by the diffusion of the group III precursor.[25] However, when we plot R_{GaAs} (at 420 °C) versus χ_{AsH3} (Figure 9a), we observe that the growth rate increases rapidly at low χ and levels off at higher χ. This demonstrates that the AsH_3 partial pressure has a large effect on the GaAs growth kinetics as well. When we plot $1/k_{GaAs}$ versus $1/\chi_{AsH3}$ (Figure 9b), it suggests a linear relation. Thus, for GaAs we have found that R_{GaAs} strongly depends on χ_{TMG} and χ_{AsH3} but that R_{GaAs} does not increase with temperature within the parameter range that was applied. The dependence of R_{GaAs} on both χ_{TMG} and χ_{AsH3} implies that the decomposition of one of these precursors is affected by the presence of the other type of precursor. It has been reported that AsH_3 enhances the decomposition of TMG in the gas phase.[26,27] It was suggested that a $(CH_3)_{3-x}$−$GaAsH_{3-y}$ complex was formed, which was subsequently decomposed at the substrate surface.

The diffusion-limited VLS growth for GaAs shows, however, that the decomposition of such a complex must be relatively fast, and we propose that it could be catalyzed at these relatively low temperatures on the surface of the nanowire or on the gold particle.[26]

Radial Growth. During the VLS growth, semiconductor material can also be deposited on the nanowire walls (this reaction is indicated as process 7 in Figure 6). This lateral growth process competes with the VLS mechanism and results in tapered wires. Such lateral, or radial, overgrowth[28] could be useful for inorganic passivation of surface states of a narrow band gap semiconductor (core) with a wide band gap material (shell).[16,29] The passivation might, for instance, enhance the mobility of the charge carriers or suppress nonradiative decay of electron−hole pairs.[30] To investigate this lateral growth, we prepared cross-sections orthogonal to the length direction of

(25) Stringfellow, G. B. *Organometallic Vapor Pressure Epitaxy: Theory and Practice*; Academic Press: Boston, 1999; 2nd ed.

(26) Reep, D. H.; Ghandhi, S. K. *J. Electrochem. Soc.* **1983**, *130*, 675−680.
(27) Den Baars, S. P.; Maa, B. Y.; Dapkus, P. D.; Danner, A. D.; Lee, H. C. *J. Cryst. Growth* **1986**, *77*, 188−193.
(28) Lauhon, L. J.; Gudiksen, M. S.; Wang, D.; Lieber, C. M. *Nature* **2002**, *420*, 57−61.
(29) Sköld, N.; Karlsson, L. S.; Larsson, M. W.; Pistol, M. E.; Seifert, W.; Trägårdh, J.; Samuelson, L. *Nano Lett.* **2005**, *5*, 1943−1947.

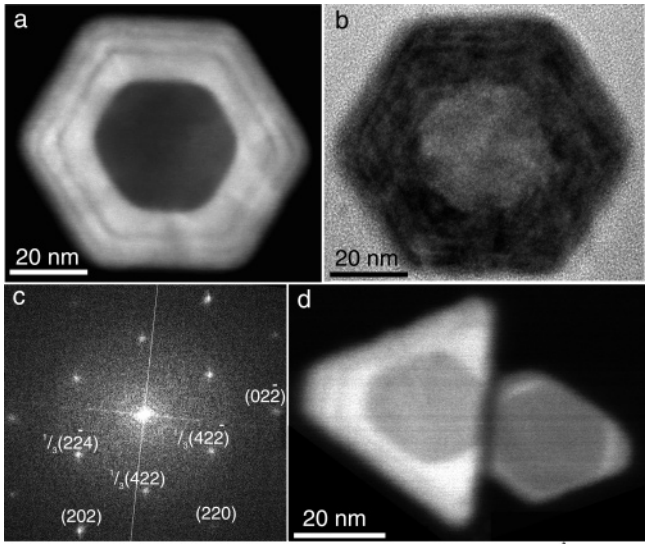

Figure 10. Cross-sectional TEM images of GaP−GaAs wires grown at 480 °C with χ_{AsH3} and $\chi_{PH3} = 1.5 \times 10^{-2}$ and $\chi_{TMG} = 7.3 \times 10^{-5}$. (a) HAADF image of a wire with a hexagonal shape that was sectioned in segment 5 (see Figure 2). (b) High-resolution TEM image of the wire in panel a. (c) Fast Fourier transform (FFT) pattern of image in panel b, displaying a [−111] zone axis pattern. The $^1/_3\{422\}$ spots are additional spots that appear due to twinning of the sample, where the twin planes are perpendicular to the viewing direction.[31] (d) HAADF image of two wires with a triangular shape. The left wire is sectioned at segment 5 and the right wire at segment 9. The hexagonal core is GaP, for the wires in these images, and the bright adlayers are GaAs, separated by darker GaP layers.

heterostructured wires grown at 480 °C. In Figure 10a, a cross-sectional HAADF TEM image of a wire with an overall hexagonal shape is shown. The contrast in the HAADF image shows that the core consists of GaP and that the brighter contrast in this image corresponds to GaAs. Judging from the HAADF contrast, we can conclude that this GaP core was overgrown by three GaAs layers separated by two GaP layers. By comparing this sequence with the HAADF image in Figure 2d, we infer that the wire is sectioned at segment 5. Since we know the growth history of each wire, we can translate a position on the wire into a total exposure time, after its formation via VLS. By using this, we estimate a radial growth rate on the nanowire side facets of 0.17 nm/s for GaAs and 0.03 nm/s for GaP. High-resolution TEM imaging (Figure 10b) of this wire shows that the lateral overgrowth is epitaxial. The FFT pattern of image 10b (see Figure 10c) indicates that this wire was grown in a ⟨111⟩ direction with {112} side facets. Note that from these images we cannot discriminate between flat {112} facets and stepped facets with an overall {112} orientation, but consisting of, for example, {111} and {113} nanofacets. In Figure 10d, a HAADF image of two wires from the same sample is presented, which have a triangular cross-sectional shape. The wires have probably been closely together during growth as can be deduced from the asymmetrical radial growth. The cores of these wires consist of GaP and were overgrown mainly by GaAs. Investigation of the EDX scans shows that three GaAs layers separated by two GaP layers have been deposited on the GaP core of the left wire and only one GaAs layer on the core of the right wire after VLS growth, showing that the left wire is sectioned at segment 5 and the right wire at segment 9. For these wires, we

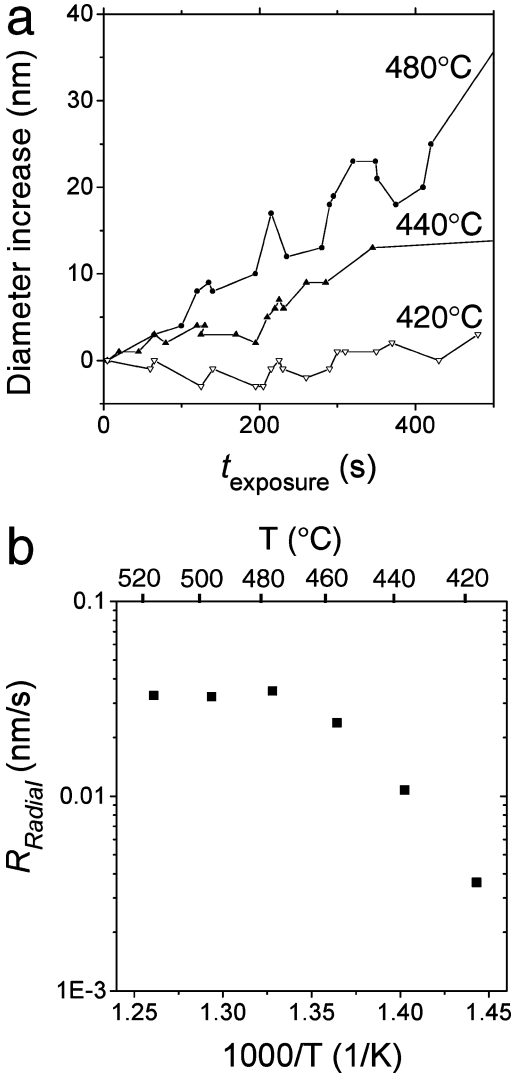

Figure 11. (a) Local diameter increase of wires, grown at 420, 440, and 480 °C, as a function of the exposure time to the gas phase, after the formation of the particular section via the VLS mechanism. The thicker parts in the wires correspond to the GaAs sections. (b) The average radial growth rate as a function of the growth temperature in a semilogaritmic plot. χ_{AsH3} and χ_{PH3} were 1.5×10^{-2}, and χ_{TMG} was 7.3×10^{-5} for these samples.

found radial growth rates of 0.13 and 0.07 nm/s for the two different ⟨112⟩ directions of GaAs and 0.02 and 0.007 nm/s for the two different ⟨112⟩ directions of GaP. Analysis of high-resolution TEM images suggests either a ⟨112⟩ or a ⟨111⟩ growth direction for these triangular wires. In total, we have investigated six wires; four wires had an overall triangular cross-sectional shape, and two wires were hexagonal. These differences in shape and growth direction will be subject of further investigation.

The lateral growth was studied more quantitatively by measuring the diameter of a wire at several positions in TEM images as, for example, in Figure 2a. In Figure 11a, the increase in wire diameter is plotted versus the exposure time for three wires grown at different temperatures. For wires grown at or below 420 °C, there was no significant increase of the wire diameter by the lateral growth. Above 440 °C, the diameter increased to a first approximation linearly with increasing exposure time. From the slope of these curves, the average radial growth rate was obtained. The periodic variations in the diameter correspond to the alternating GaP−GaAs structure; the GaAs

(30) van Vugt, L. K.; Veen, S. J.; Bakkers, E. P. A. M.; Roest, A. L.; Vanmaekelbergh, D. A. M *J. Am. Chem. Soc.* **2005**, *127*, 12357−12362.
(31) Pashley, D. W.; Stowell, M. J. *Philos. Mag.* **1963**, *8*, 1605−1632.

segments had, for all temperatures, a larger diameter than the GaP sections. In Figure 11b, the radial growth rate, R_{radial}, is plotted logarithmically versus 1000/K (Arrhenius plot). The growth rate increases from 0.005 to 0.035 nm/s in the temperature range of 420−480 °C and is independent of temperature for the temperature range of 480−520 °C. This demonstrates that the radial growth changes from a thermally activated process at lower temperatures to a diffusion-limited process at higher temperatures. The differences in growth rates, obtained from the cross-sectional studies as compared to the measurements in Figure 11, might be explained by the fact that for the latter studies, we determined the diameter from a projection view. This could induce errors since the overall shape might be triangular. From the cross-sectional samples, grown at 480 °C, we found that mainly GaAs (but also some GaP) is deposited on the nanowire walls. These results demonstrate the close competition between VLS and radial growth for the GaAs precursors, where radial deposition starts to limit VLS growth above 460 °C. Because hardly any GaP is deposited on the nanowire surface below 500 °C, the precursors for GaP are not depleted, and a growth rate as high as 20 nm/s can be obtained for the VLS growth of GaP. Above 500 °C, the kinetic barrier for GaP film deposition has been overcome, and this reaction competes with the VLS growth.

Conclusions

We have shown that the nanowire growth dynamics can be studied in great detail by using heterostructures. We have demonstrated that the gold particle effectively catalyzes the decomposition of PH_3, which is the rate-limiting factor for the growth of GaP. For GaAs, we have found that mass transport controls the growth. We have shown that the chemistry of the group V precursors is an important element in the VLS growth of GaP and GaAs, although we applied rather high V/III ratios (between 10 and 700) in our experiments as compared to others studied, in which the growth was controlled by the group III precursor. In this context, it is important to stress the role of the SiO_2 substrate in our experiments, yielding different kinetics for dissociation and diffusion processes and preventing thin film growth as compared to studies where III−V substrates were used. A next step would be to investigate whether the formation of twin boundaries in [111]-oriented wires could be affected by growth parameters.

Acknowledgment. We acknowledge M. Kaiser and R. G. R. Weemaes for FIB preparation of the cross-sections of the nanowires.

JA057157H